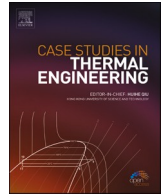




ELSEVIER

Contents lists available at [ScienceDirect](https://www.sciencedirect.com)

Case Studies in Thermal Engineering

journal homepage: <http://www.elsevier.com/locate/csite>

Computational fluid dynamics model for a variable conductance thermosyphon

Cho-Ning Huang^a, Kuan-Lin Lee^b, Calin Tarau^b, Yasuhiro Kamotani^a,
Chirag R. Kharangate^{a,*}

^a Department of Mechanical and Aerospace Engineering, Case Western Reserve University, 10900 Euclid Avenue, Cleveland, OH, 44106, USA

^b Advanced Cooling Technologies, Inc., 1046 New Holland Ave., Lancaster, PA, 17601, USA

ARTICLE INFO

Keywords:

Variable conductance heat pipe
CFD
Two-phase flow
Diffused interface

ABSTRACT

A variable conductance thermosyphon is a unique type of heat pipe that responds passively to changes in thermal environment because of the presence of non-condensable gas (NCG). In this study, we develop a computational fluid dynamics (CFD) model to predict the behavior of a cylindrical-shaped variable conductance thermosyphon in the vertical orientation for a range of evaporator-side operating temperatures between 66.70 °C and 87.32 °C. Experiments are performed on a variable conductance thermosyphon that is made of a 262 mm long stainless steel tube with an outer diameter of 9.5 mm and a wall thickness of 0.92 mm. The working fluid is methanol and the NCG is argon. The model is able to predict the fluid flow and heat transfer in the fluid domain and the conjugate heat transfer to the solid wall domain. Experimental thermocouple data for both forced convection and natural convection test cases show temperature remaining almost uniform in the adiabatic section and dropping rapidly across the vapor/NCG interface between the vapor and NCG. This behavior of wall temperature change was also captured accurately by the CFD model, evidenced by MAEs of 3.09% and 3.52% for forced and natural convection test cases, respectively.

1. Introduction

For the success of future NASA's long-duration space missions, significant challenges in thermal management need to be addressed. Two-phase devices provide many benefits in heat transfer and reduction in mass over traditional single-phase counterparts [1]. Therefore, they can be critical to increasing the duration and extending power utilization during space missions. One such two-phase device is a heat pipe which has excellent heat transfer capabilities. They can transfer heat over long distances with minimum temperature drops and no need for external power [2]. A simple type of heat pipe in which gravity assists the condensed liquid returning to the evaporator from the condenser is a two-phase closed thermosyphon. In a two-phase closed thermosyphon, working fluid, which is originally in a liquid state, is vaporized by the heat input to the evaporator side. The vapor passes through the adiabatic section and condenses on the condenser walls, releasing the latent heat [3]. Due to gravity, the condensed liquid returns back to the evaporator side and is re-vaporized. This internal phase-change and circulation are the mechanisms of operation of the device. The result is a large amount of heat transfer between the evaporator and the condenser without requiring a significant temperature difference.

* Corresponding author.

E-mail address: chirag.kharangate@case.edu (C.R. Kharangate).

URL: http://engineering.case.edu/emaefaculty/Chirag_Kharangate (C.R. Kharangate).

<https://doi.org/10.1016/j.csite.2021.100960>

Received 4 February 2021; Received in revised form 16 March 2021; Accepted 20 March 2021

Available online 31 March 2021

2214-157X/© 2021 The Author(s). Published by Elsevier Ltd. This is an open access article under the CC BY-NC-ND license

(<http://creativecommons.org/licenses/by-nc-nd/4.0/>).

Nomenclature

A	cooling area
C	heat transfer coefficient factor
c_p	specific heat
D	diameter
d_{12}	binary diffusion coefficient
Gr	Grashof number
g	gravity
H_{fg}	latent heat
h	heat transfer coefficient
k	thermal conductivity
L	length
M	molecular mass
m	mass
\dot{m}	mass flow rate
MAE	mean absolute error
Nu	Nusselt number
n	heat transfer coefficient constant
P	pressure
Pr	Prandlt number
R_{mixed}	mixed gas constant
Re	Reynolds number
r	radial coordinate
T	temperature
u	velocity
V	volume
z	axial coordinate

Greek Symbol

α	thermal diffusivity
ρ	density
μ	dynamic viscosity
φ	concentration

Subscripts

air	air
avg	average
c	cooling
$cond$	condensation
D	diameter
exp	experiment
f	saturated liquid
g	saturated vapor
L	cooling length
sat	saturation state
w	wall
∞	free flow

Unique to space missions is another need to operate in both cold and hot environments during the missions [4]. This is where another of a heat pipe comes in which is the variable conductance heat pipe (VCHP) [5]. In a VCHP, in addition to the working fluid, a non-condensable gas (NCG) is included inside the closed loop. The advantage is that the NCG allows VCHP to respond passively to changes in the thermal environment. When the environmental temperature rises, the evaporator side temperature increases, increasing the internal pressure and compressing the NCG to increase the condenser area, in turn making the VCHP more conductive. In contrast, it becomes less thermally conductive when the environmental temperature drops because as the evaporator side temperature decreases there is a decrease in internal pressure and expansion in the NCG that reduces the condenser area. This design minimizes the changes in the evaporator-side temperature even if there are large changes to input heat.

1.1. Literature review

A number of experimental investigations on heat pipes have been reported in the last 5 decades. In 1971, Lee and Mital [3] performed a series of experiments to investigate the heat transfer performance of a two-phase closed thermosyphon. Water and Freon-11 were used as the working fluids. The authors investigated the impact of several parameters including the amount of the working fluid, the ratio of heated length to cooled length, the operating pressure, the heat flux, and the working fluid. Maximum heat transfer rates predicted by their theoretical analysis showed good agreement with the experimental results. Shirashi et al. [6] studied the heat transfer characteristics of a closed two-phase thermosyphon experimentally and developed a simple mathematical model to predict its performance. Water, ethanol and Freon 113 were used as the working fluids. Shirashi et al. tested the effects caused by different working fluid inventories, operating temperatures, and heat fluxes. A mathematical model was developed based on these experimental results. A good agreement was observed between the mathematical model and the experimental results. Critical heat flux (CHF) behavior in a closed two-phase thermosyphon was studied by Imura et al. [7]. The effects of the inner diameter, working fluid and its filling ratio, heated length, and working temperature on the CHF were studied in their work. The working fluids used in the experiments were Freon 113, water and ethanol. They developed a correlation which showed good agreement in predicting the experimental data with $\pm 30\%$ accuracy. Akbarzadeh and Johnson [8] performed a series of experiments to investigate the minimum needed temperature difference between evaporator and condenser for the operation of a closed two-phase thermosyphon. In their study, R11, R22, and water were used as the working fluids. From the results of these experiments, Akbarzadeh and Johnson established the minimum temperature differences required to trigger and sustain continuous boiling. In addition, they proposed a method to improve the performance of the heat pipe at low-temperature differences between the evaporator and condenser. Experiments were performed by Hashimoto and Kaminaga [9] to examine the heat transfer behaviors in the condenser region by using two different types of test sections. The first was a fixed-diameter test section, whereas the second had a large-diameter evaporator compared to the condenser, to reduce entrainment. The working fluids were water, R113 and ethanol. In their study, Hashimoto and Kaminaga proposed a new correlation for heat transfer coefficient for the heat pipe including the effect of liquid entrainment. Noie [10] studied experimentally, the influence of three parameters of a closed two-phase thermosyphon. The parameters investigated in this study were the input heat transfer rates ($100 < \dot{Q} < 900\text{W}$), the working fluid filling ratios ($30\% \leq \text{FR} \leq 90\%$), and the evaporator lengths (aspect ratio equals 7.45, 9.8, and 11.8). Water was used as the working fluid. The experimental boiling heat transfer coefficient data were compared with correlations and optimum filling ratios and aspect ratios were selected. Jouhara and Robinson [11] tested experimentally of the effect of different working fluids on the heat transfer performance of small diameter two-phase closed thermosyphon. The inner radius of the cooper thermosyphon was 6 mm and its length was 200 mm which contains a 40-mm evaporator and a 60-mm condenser. Water, FC-84, FC-77 and, FC-3283 was used as the working fluids. From their study, the results showed that the water-charged thermosyphon has good agreement comparing with prior correlations and theories. Moreover, water-charged thermosyphon also outperformed the other working fluids in both effective thermal resistance and maximum heat transfer capability. The most recent study on a two-phase thermosyphon was reported by Gedik [12] where they tested the thermal performance, under different operating conditions, experimentally. The thermosyphon was tested under different rates of cooling water flow (10, 20, 30 L/h), inclination angles (30° , 60° , and 90°), and heat inputs (200, 400, and 600 W). The working fluid was water in the experiments. The results showed that the efficiency of the thermosyphon is sensitive to inclination and heat input rates.

Besides the experimental studies discussed above, many researchers have used a numerical approach to investigate the thermosyphon heat pipes. Harley and Faghri [13] built a two-dimensional model to simulate the heat transfer through the wall of the thermosyphon and the falling condensate liquid film. A quasi-steady, Nusselt-type analysis was used to model the falling film. Experimental data of the low-temperature thermosyphon was used to validate the model and a good agreement was observed in their study with experiments. A CFD model was developed by Legierski et al. [14] to simulate the effects of liquid evaporation and condensation inside heat pipes. The simulation results were compared with those from experiments. Water was used as the working fluid. The effective thermal conductivity and temperature increase in the transient state during startup was investigated in their study. Jiao et al. [15] developed a numerical model to study the effect of filling ratio on the steady-state heat transfer performance of a vertical two-phase closed thermosyphon. The working fluid in their study was nitrogen. Predicted results were compared with those by other heat transfer empirical correlations from literature, and a range of filling ratio was proposed based on their analysis and comparison. Alizadehdakheel et al. [16] developed a CFD model to simulate the flow motion and heat transfer phenomenon in a two-phase thermosyphon. In their study, ANSYS FLUENT was used for the simulation, and a volume of fraction (VOF) multi-phase model was applied. CFD results were compared with experimental data, and good agreement was observed between simulation and experimental data. The authors concluded that CFD can be a useful tool to model a thermosyphon. Reported by Fadhl et al. [17], a CFD model was built to investigate the thermal and hydrodynamic behaviors of a two-phase thermosyphon. In their study, Fadhl et al. also used the VOF model in ANSYS FLUENT. The working fluid was water and the results showed good agreement between CFD and experimental data. The relative errors of condenser, adiabatic, and evaporator average temperatures were 1.9%, 9.9%, and 7.9%,

respectively. In another study, Fadhil et al. [18] examined the application of the CFD model by testing different working fluid, R134a, and R404a. Simulation results were compared with experimental data and good agreements were obtained between them. The authors concluded that the model can be applied generally to other closed two-phase thermosyphons. Shabgard et al. [19] developed a two-dimensional numerical model to simulate the thermal and hydrodynamic behavior of a thermosyphon with various working fluid filling conditions. The working fluid used in their study was water. The model was validated by comparing with experimental data. The authors concluded that the optimal filling ratio has the following characteristics: short response time and low thermal resistance. An optimal thermosyphon is recommended to have additional working fluid to ensure a stable working condition. Recently, we are also seeing some interests on utilizing nanofluids inside the thermosyphons to enhance their thermal performance. In one study, Sichamnan et al. [27] studied two-phase flow patterns occurring inside a closed thermosyphon with two internal diameters, 7 mm and 25.2 mm. The working fluid was de-ionized water mixed with silver nanoparticles. Different inclined angles and evaporator temperatures were tested in their study. They observed various boiling regimes, including bubbly, slug, annular, churn, and stratified flows. The results showed that the flow patterns are affected to a good degree by the inclined angle leading to different heat transfer rates. Ramezanizadeh et al. [21] investigated a thermosyphon with Ni/Glycerol-water nanofluid at three concentration levels of 0.416, 0.625 and 1.25 g/lit. The results showed that the nanofluid thermosyphon provided significant heat transfer improvement over a copper heat exchanger. In another study, Ramezanizadeh et al. [22] performed a comprehensive review of literature utilization nanofluids in thermosyphons that included a discussion on the types of nanoparticles, working fluids, and concentration levels. They showed that nanofluids are able to enhance the efficiency of the thermosyphons as they provide an increased effective thermal conductivity. In a recent study, a comprehensive review of several published experimental and theoretical studies on the two-phase closed thermosyphons was performed by Jafari et al. [20]. The authors discussed the parameters which affect thermosyphon heat transfer performance such as the geometry, the inclination angle, the filling ratio, the working fluid, the operating temperature, and the operating pressure.

While a lot of studies have investigated fluid flow and heat transfer in two-phase thermosyphons, not a lot of work has been done on

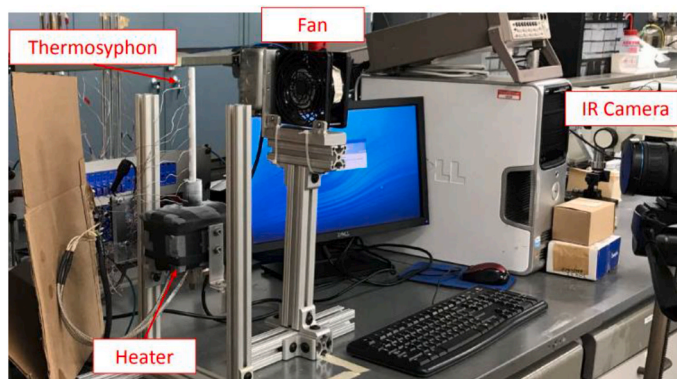
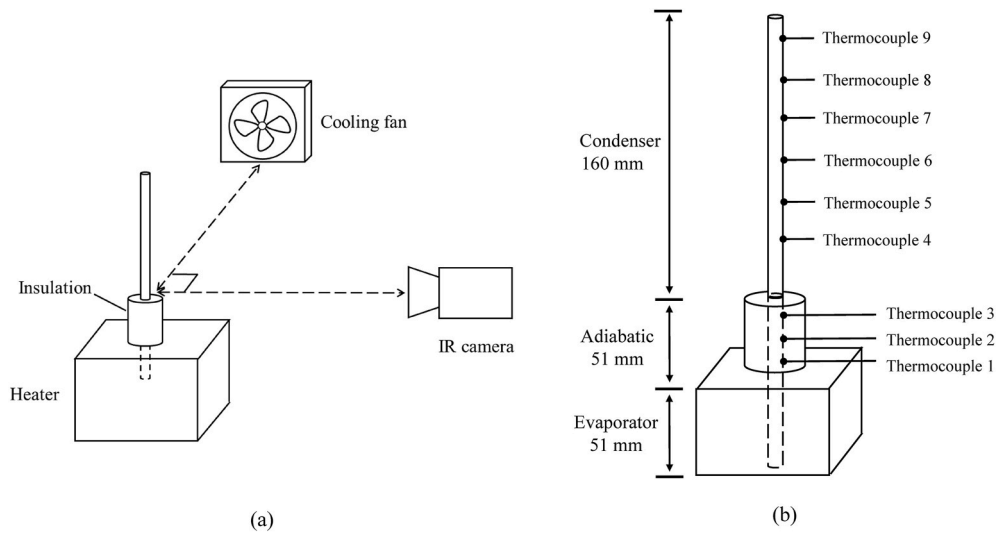


Fig. 1. (a) Schematic of the complete experimental configuration. (b) Detailed information of the thermosyphon. (c) Photograph of the experimental setup.

Table 1
The locations of the thermocouples.

Number of thermocouple	Distance from the heat block (mm)
1	11.1
2	36.7
3	50.8
4	95.3
5	120.7
6	139.7
7	162.0
8	192.1
9	204.8

variable conductance (gas-charged) thermosyphons that are types of VCHPs. In 1973, Rohani and Tien [23] analyzed a gas-loaded heat pipe numerically where the effect of gas-vapor diffusion phenomenon was included in the analysis. Ponnappan [24] investigated heat pipes with charged non-condensable gas and performed some experiments to observe the thermal behaviors of the VCHP. Harley and Faghri [25] developed a mathematical model to analyze transient gas-loaded heat pipes. Their model successfully predicted the complete behavior of the heat pipe with the location of the NCG front. In another study, Lee et al. [26] proposed a 2D CFD model to predict the behavior of a variable conductance planar heat pipe. In their model, they used a sharp interface assumption to simulate the NCG-vapor interface. The working fluid was ethanol and the non-condensable gas was nitrogen. To validate this model, experiments were performed for the same operating conditions as the numerical simulations. The authors concluded that this model was able to predict the NCG interface location and the operating temperature accurately for a range of operating conditions. A recent study about heat pipe charged with NCG was done by Enke et al. [28]. Authors developed a mathematical model and validated it with experimental data from axially-grooved aluminum-ammonia heat pipe. Good agreement was obtained in this study. Other than these studies, not many good computational investigations for variable conductance thermosyphons are available. That is even after VCHPs being so commonly used now across many industrial applications. Therefore, a deeper understanding and new modeling efforts are needed in order to investigate the fluid flow and heat transfer inside a variable conductance thermosyphon.

1.2. Objective

As discussed earlier, not many CFD attempts have been made at simulating a variable conductance thermosyphon configuration. In addition, the only study that developed a full CFD model utilized a sharp interface assumption between the vapor and the NCG domain [26], which is not accurate in capturing the diffusion occurring between the two phases. In this study, we plan to develop a new computational framework to predict the behavior in a cylindrical variable conductance thermosyphon in the vertical orientation for a range of evaporator-side operating temperatures by including a diffused interface modeling strategy to accurately capture the heat transfer and fluid flow. The CFD model will be developed utilizing an in-house code in Fortran to predict the fluid flow and heat transfer in the fluid domain and the conjugate heat transfer to the solid wall domain. Experiments will also be performed in the same configuration as the planned CFD simulations, and the results will be used to validate the CFD model performance.

2. Experimental methods

2.1. Experiment configuration

The experimental configuration schematic of the gas-charged thermosyphon is shown in Fig. 1(a). The apparatus consists of a heater, a thermosyphon, a cooling fan, and an IR camera. The thermosyphon, placed vertically, consists of a 262- mm long stainless steel 304 tube with an outer diameter of 9.5 mm and a wall thickness of 0.92 mm. As shown in Fig. 1(b), the evaporator section of the thermosyphon includes a heater box with a maximum power output of 400 W. The length of the evaporator is 51 mm. This is followed by a 51 mm long adiabatic section. The adiabatic section is insulated to prevent any heat loss to the ambient. The last section on the top is the condenser section with a total length of 160 mm. A fan is placed in front of the condenser section of the thermosyphon to provide air-cooling for the forced convection test cases. An air flow meter (anemometer) is used to measure the air flow velocity which has an accuracy of $\pm 5\%$. The velocity of the cooling air flow is calculated by averaging ten data points. The fan is turned off for the natural convection test runs. Nine thermocouples were attached to the wall of the thermosyphon to measure the axial wall temperature distribution in the adiabatic and the condenser sections. The exact locations of thermocouples are listed in Table 1. The accuracy of the thermocouples is ± 1.0 °C. In addition, an Infrared (IR) camera was also used to capture the wall temperature contours of the

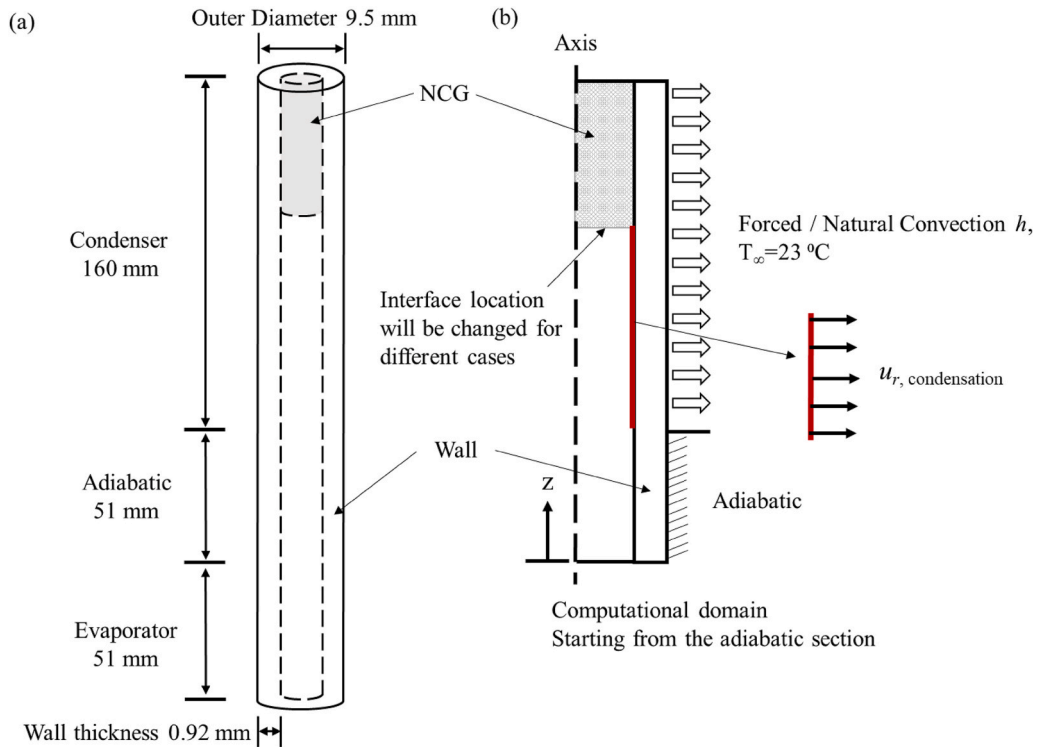


Fig. 2. (a) Cylindrical domain of the computational model. (b) 2-D axisymmetric domain modeled in the present study and boundary conditions.

thermosyphon for qualitative comparison. The accuracy of the IR camera measurement is $\pm 5\%$. Fig. 1(c) shows a photographic image of the experimental setup including the cooling fan, the thermosyphon, and the IR camera.

2.2. Operation condition

The working fluid used for the tests is methanol with a total volume of 3 ml and the non-condensable gas (NCG) used is argon with a total mass of 4.86 ± 0.22 mg. Two sets of experiments were performed, one with the fan on for forced convection, and another one with the fan off for natural convection. Forced convection experiments were conducted at three operating temperatures of 66.70, 77.02, and 86.92°C and a fixed air velocity of 1.07 ± 0.14 m/s measured with the use of an anemometer and ambient temperature, $T_\infty = 23.1^\circ\text{C}$. Natural convection experiments were conducted at three operating temperatures of 68.00, 78.04, and 87.32°C and ambient temperature $T_\infty = 23.0^\circ\text{C}$. Gases that do not condense to liquid state within the operating conditions of the heat pipe operation can be considered as NCG. Since the boiling point of Ar (-185.7°C at atmospheric pressures) is much lower than the heat pipe operating range, it can be used as NCG. The operating temperatures stated above and what will be used throughout this study were estimated by taking the average wall temperature of the thermocouples located in the adiabatic section.

3. Computation methods

3.1. Computational domain

A computational fluid dynamics (CFD) model was developed to simulate the experimental test setup of the gas-charged thermosyphon described in Section 2. This was an in-house programming code written and solved in Fortran. Fig. 2(a) shows the three-dimensional (3D) geometry of the gas-charged thermosyphon, and Fig. 2(b) shows the details of the two-dimensional (2D) axisymmetric computational domain used to simulate the fluid flow and heat transfer. The evaporator section was not modeled and so the 2D domain consisted of a thin solid wall with the adiabatic section and the condenser section. In the CFD model, the flow is assumed to be

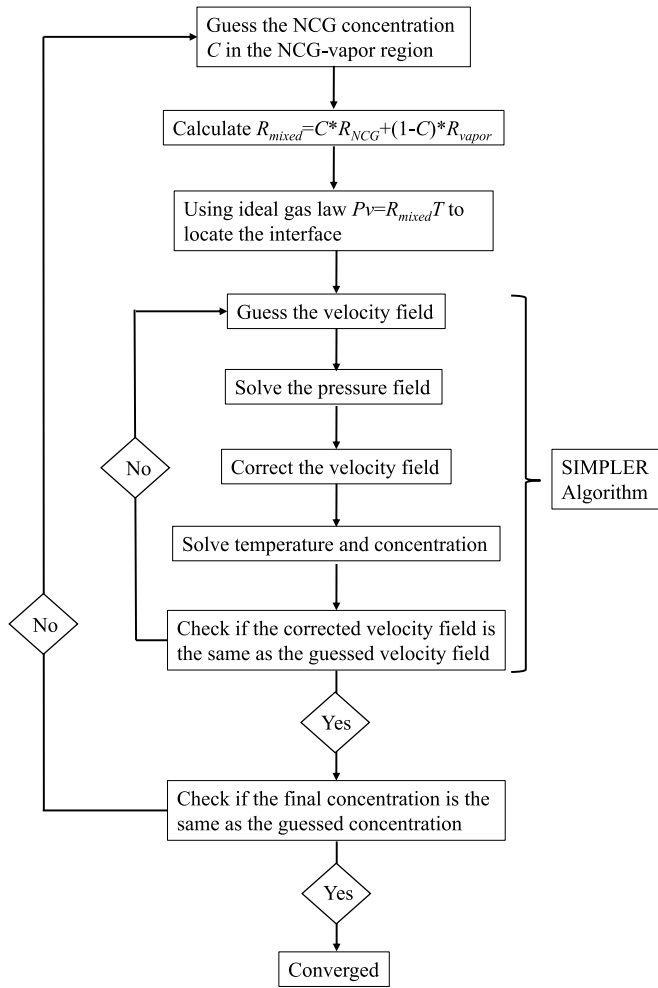


Fig. 3. Iterative procedure used to compute the NCG concentration in combination with the conservation equations.

axisymmetric and two-dimensional which is a reasonable assumption for simulating thermosyphon in the vertical orientation. While the thermosyphon will include three phases: working fluid vapor phase, working fluid liquid phase and NCG phase, we only model two gas phases in this study, including the working fluid vapor phase and the NCG phase. A two-phase diffused interface separating the NCG and the working fluid vapor phases were also modeled in the CFD. Condensation mass transfer correlations are used to estimate the rate of vapor phase-change and heat transfer at the cooling wall without actually modeling the liquid film. The liquid film was not modeled in the CFD due to the following reasons. Firstly, including three phases along with two types of interfaces, one diffused interface between the vapor and NCG and one sharp interface between the vapor and liquid, complicates the CFD model development effort significantly. Secondly, we verified from Ref. [29], that the thickness of the liquid film for all the test cases at the end of the condenser section was less than 1.6% of the inner radius. Therefore, its effect on the heat transfer to the computational domain is insignificant. This was verified in the CFD by adding a thin low-conductivity zero-velocity fluid domain in the domain near the wall and comparing the heat transfer results with and without the liquid film. Thirdly, a similar approach to this was followed in the study by Lee et al. [26] where they successfully modeled and investigated a rectangular configuration of the VCHP with only the vapor and NCG phases, neglecting the effect of the liquid phase.

Table 2
The finalized interface locations of each tested case.

Forced convection		
Operating T (°C)	T _{avg} (°C)	x/L
66.7	24.15	0.611
77.02	32.17	0.734
87.92	47.59	0.807
Natural convection		
Operating T (°C)	T _{avg} (°C)	x/L
68.00	28.83	0.634
78.04	39.44	0.687
87.32	51.76	0.77

3.2. Governing equations

For this two-phase flow simulation, the flow and heat transfer are governed by the continuity equation, momentum equations, energy equation and diffusion equation. Using the incompressible and axisymmetric assumptions mentioned above, the governing equations can be simplified as follows:

The continuity equation is given by:

$$\frac{1}{r} \frac{\partial}{\partial r} (ru_r) + \frac{\partial u_z}{\partial z} = 0, \tag{1}$$

and

$$\dot{m}_{\text{vapor}} = \dot{m}_{\text{cond}} = \frac{hA_c(T_{\text{sat}} - T_{\text{air}})}{H_{fg}}. \tag{2}$$

Momentum conservation equations are given by:

$$\rho \left(u_r \frac{\partial u_r}{\partial r} + u_z \frac{\partial u_r}{\partial z} \right) = - \frac{\partial P}{\partial r} + \mu \left[\frac{1}{r} \frac{\partial}{\partial r} \left(r \frac{\partial u_r}{\partial r} \right) - \frac{u_r}{r^2} + \frac{\partial^2 u_r}{\partial z^2} \right]. \tag{3}$$

and

$$\rho \left(u_r \frac{\partial u_z}{\partial r} + u_z \frac{\partial u_z}{\partial z} \right) = - \frac{\partial P}{\partial z} - \rho g + \mu \left[\frac{1}{r} \frac{\partial}{\partial r} \left(r \frac{\partial u_z}{\partial r} \right) + \frac{\partial^2 u_z}{\partial z^2} \right]. \tag{4}$$

The energy conservation equation is given by:

$$\rho c_p \left(u_r \frac{\partial T}{\partial r} + u_z \frac{\partial T}{\partial z} \right) = \alpha \nabla^2 T, \tag{5}$$

The diffusion equation is given by:

$$u_r \frac{\partial \varphi}{\partial r} + u_z \frac{\partial \varphi}{\partial z} = d_{12} \nabla^2 \varphi, \tag{6}$$

Here, ρ is the density of the fluid, u_r is the radial velocity, u_z is the axial velocity, P is the pressure of the flow field, T_{sat} is the saturation temperature, T_{air} is the ambient temperature, μ is the dynamic viscous coefficient, \dot{m} is the condensation mass flow rate, H_{fg} is the latent heat of the fluid, h is the heat transfer coefficient, A_c is the cooling area, φ is the concentration, and d_{12} is the binary diffusion coefficient. An unknown here is the diffusion coefficient, d_{12} . Above the two-phase interface, methanol and argon are mixed. Since the diffusion rate between methanol and argon cannot be directly estimated from the experiments, it is crucial to find a way to estimate the diffusion coefficient of the mixture theoretically. From Ref. [30], it was shown that the binary diffusion coefficient between two gases is only dependent on the molecule mass of the mixed gases and is given as follows:

Table 3
Constants of equation (10) for the circular cylinder in the cross flow [18].

Re _D	C	n
0.4–4	0.989	0.330
4–40	0.911	0.385
40–4000	0.683	0.466
4000–40,000	0.193	0.618
40,000–400,000	0.027	0.805

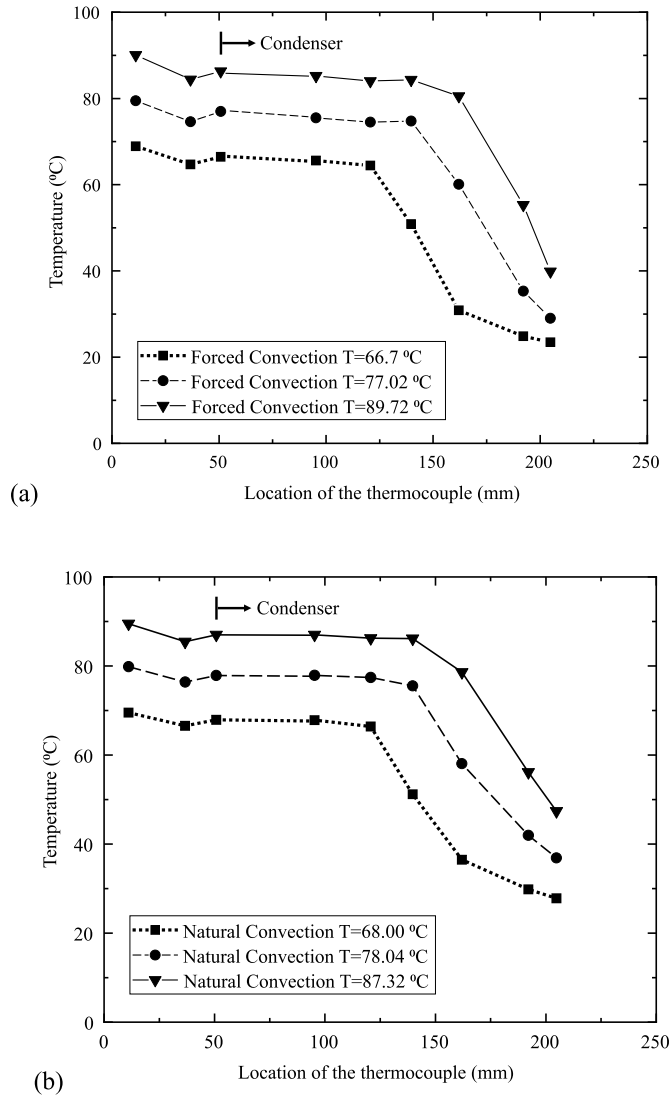
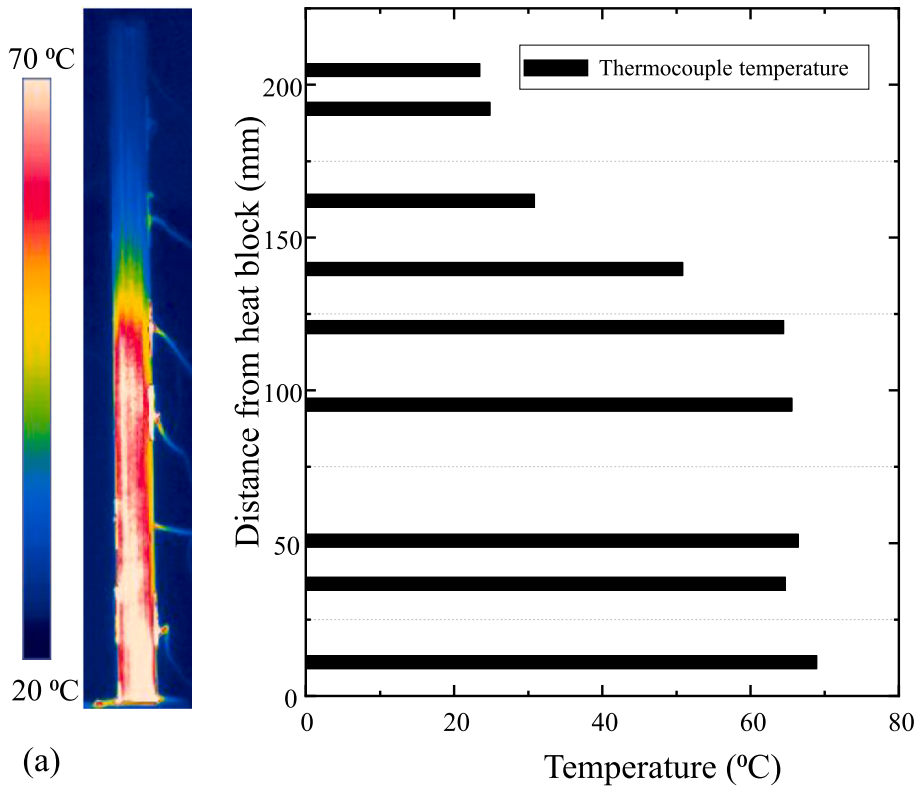


Fig. 4. (a) Experimental thermocouple data for forced convection cases. (b) Experimental thermocouple data for natural convection cases.

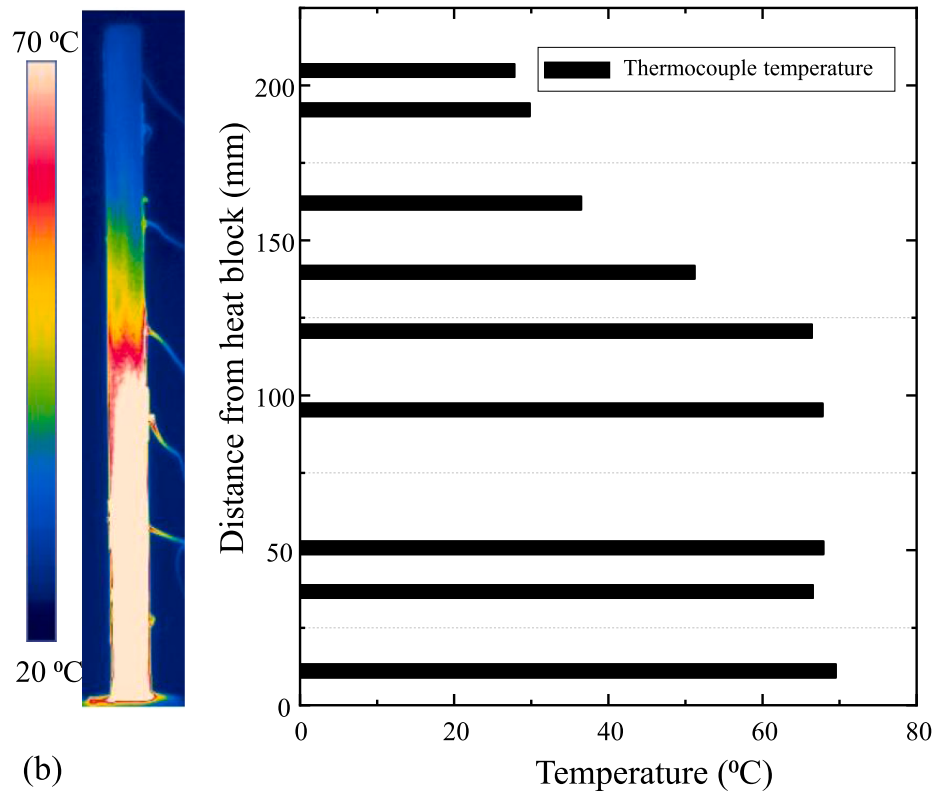
$$d_{12} \propto \left(\frac{1}{M_1} + \frac{1}{M_2} \right)^{0.5} \tag{12}$$

where M is the molecule mass. Therefore, to estimate the diffusion coefficient for a mixed gas combination of Ar as NCG and methanol as the working gas, we can use the diffusion coefficient based on Ar and O_2 . O_2 has the same molecule mass as methanol, and the d_{12} for this mixture was available in Ref. [30].

To correctly model the variable conductance thermosyphon, another calculation that needs to be done is estimating the location of the interface between the vapor and the NCG domains. While the mass fraction of the two gas species, methanol and argon, are known, it cannot be directly used to determine this location as that also depends on the temperature of the working fluid. An iterative procedure shown in Fig. 3 is used to compute the interface location in combination with the CFD modeling of the mass, momentum, and energy conservation equations. We start by guessing a value for the NCG concentration and calculating the corresponding mixed gas constant, R_{mixed} in the NCG domain. Next, using the ideal gas law, $P_{sat}V = mR_{mixed}T_{avg}$, we determine the volume of the NCG. T_{avg} is averaged by the wall temperature in the NCG region from the experimental data. With the volume fraction computed, the location of the interface is now set. The governing equations for mass, momentum, energy, and concentration are solved in the computational domain to calculate the velocity, temperature, and concentration distributions. The final computed mass concentration is then compared with the guessed concentration value. If they match with each other, the solution is converged. If not, we update the guessed value of the concentration using the bisection method and follow the same steps discussed above until we get a converged solution. As shown in Table 2, the interface location for each test case was computed and was seen to depend strongly on the operating temperature



(a)



(b)

Fig. 5. Comparison of IR image temperature data and thermocouple data for (a) forced convection test case with operating temperature of 66.7 °C and (b) natural convection test case with operating temperature of 68 °C.

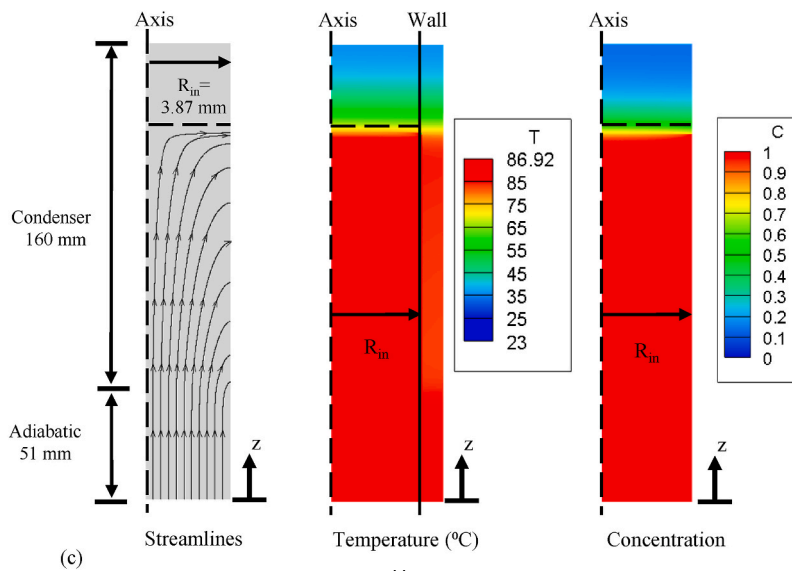
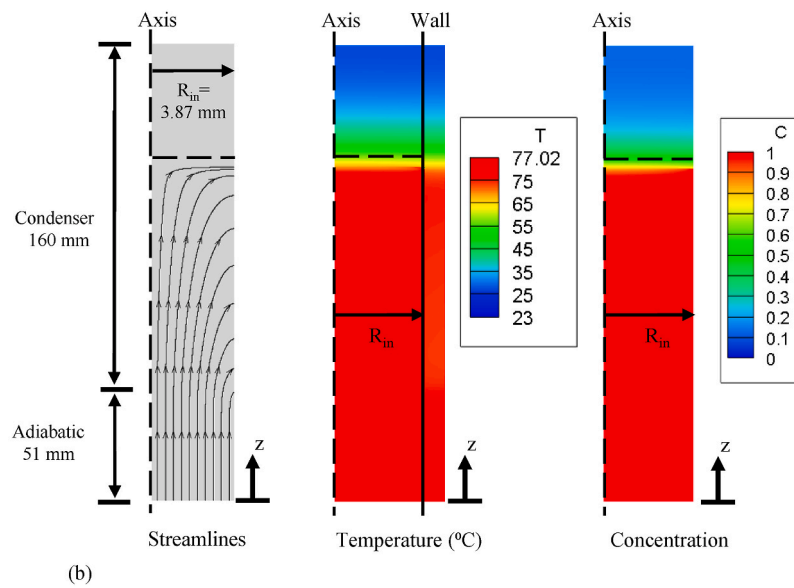
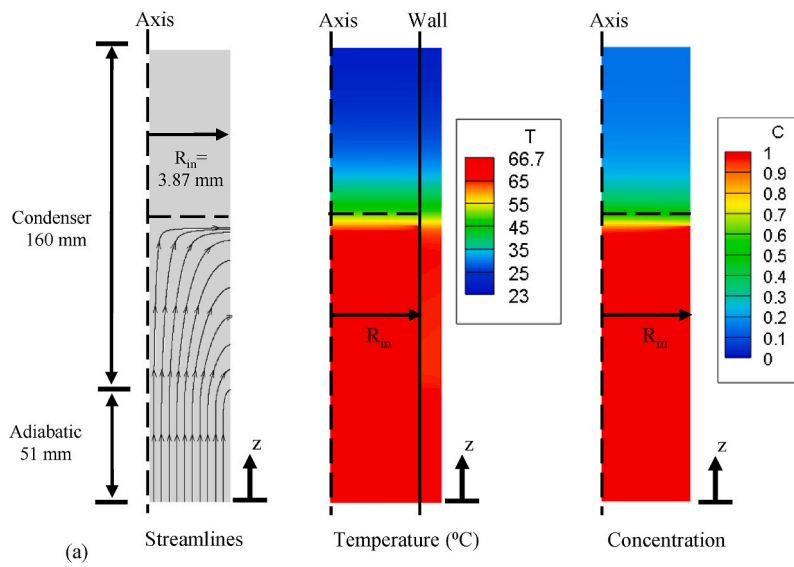


Fig. 6. CFD simulation results for forced convection tests with (a) working temperature of 66.7 °C, (b) working temperature of 77.02 °C, and (c) working temperature of 86.92 °C.

of the working fluid, methanol.

3.3. Boundary conditions

While the liquid phase is not modeled, condensation mass transfer is simulated in this study. Mass transfer at the cooling wall is simulated using an outward radial velocity boundary condition, u_{cond} , at the vapor-solid interface as shown in Fig. 2(b). The condensing mass flow rate, \dot{m}_{cond} , is given as

$$\dot{m}_{\text{cond}} = \frac{\bar{h}_L A_c (T_{\text{sat}} - T_w)}{H_{fg}}, \quad (7)$$

and the corresponding velocity is given as

$$u_{\text{cond}} = \frac{\bar{h}_L (T_{\text{sat}} - T_w)}{\rho_f H_{fg}}, \quad (8)$$

where the average heat transfer coefficient, \bar{h}_L , is calculated using the correlation for condensation heat transfer given by Ref. [29]:

$$\bar{h}_L = 0.943 \left[\frac{\rho_f g (\rho_f - \rho_g) H_{fg} L_c^3}{\mu_f k_f (T_{\text{sat}} - T_w)} \right]^{1/4}, \quad (9)$$

The axial velocity is set to zero at the two-phase interface between the vapor and the NCG phase. This assumption is reasonable since the flowing vapor cannot pass through the interface and enter the NCG region. An adiabatic condition is applied to the insulated wall section. At the inlet to the variable conductance thermosyphon, a pressure boundary condition is applied. This pressure was based on the saturation pressure, P_{sat} , corresponding to the working temperature of methanol. For the external wall cooling condition, the heat transfer rate was estimated based on the empirical correlation for flow around a cylinder by Hilpert [31]:

$$\overline{Nu}_D \equiv \frac{\bar{h}D}{k_{\text{air}}} = C Re_D^n Pr^{1/3}, \quad (10)$$

and was applied in forced convection test cases where constant C and n are listed in Table 3. An average Nusselt number estimated by Ede [32] based on the height of the cylinder was used to estimate the heat transfer rate in the natural convection test cases:

$$\overline{Nu}_L \equiv \frac{\bar{h}L}{k_{\text{air}}} = \frac{4}{3} \left[\frac{7GrPr^2}{5(20 + 21Pr)} \right]^{1/4} + \frac{4(272 + 315Pr)L}{35(64 + 63Pr)D} \quad (11)$$

where Pr is the Prandtl number and Gr is the Grashof number. All the boundary conditions used in this study have been summarized in Fig. 2(b).

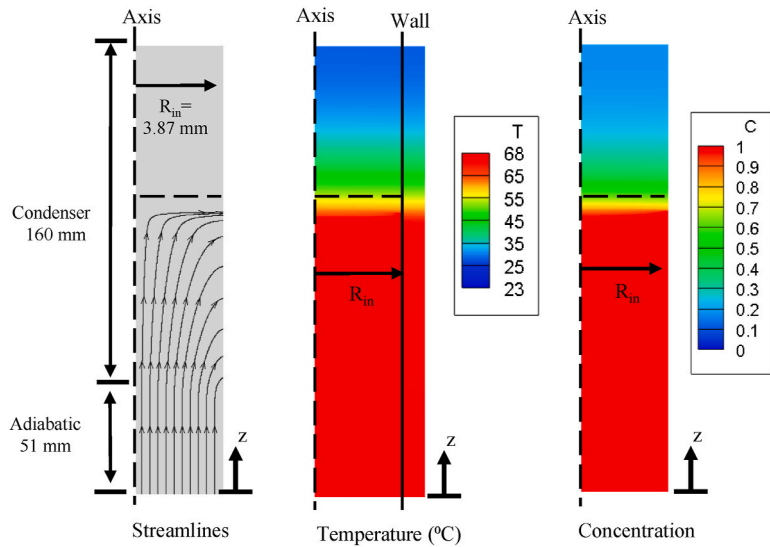
3.4. Algorithm and grid independence study

This work employs the SIMPLER algorithm [33] to solve the governing equations with a uniform staggered mesh utilized in the complete computational domain. The power-law scheme was applied when discretizing the governing equations. The process of solving the whole problem is shown in Fig. 3. Mesh independence is investigated and confirmed.

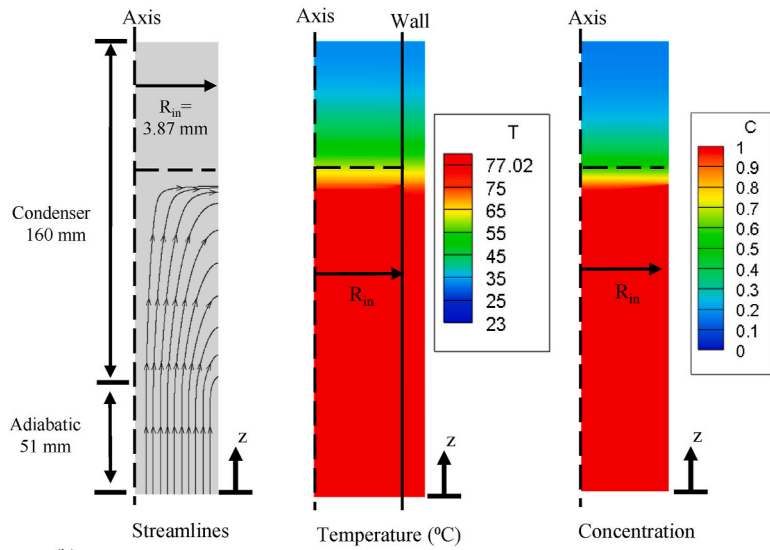
4. Results and discussion

4.1. Experimental results

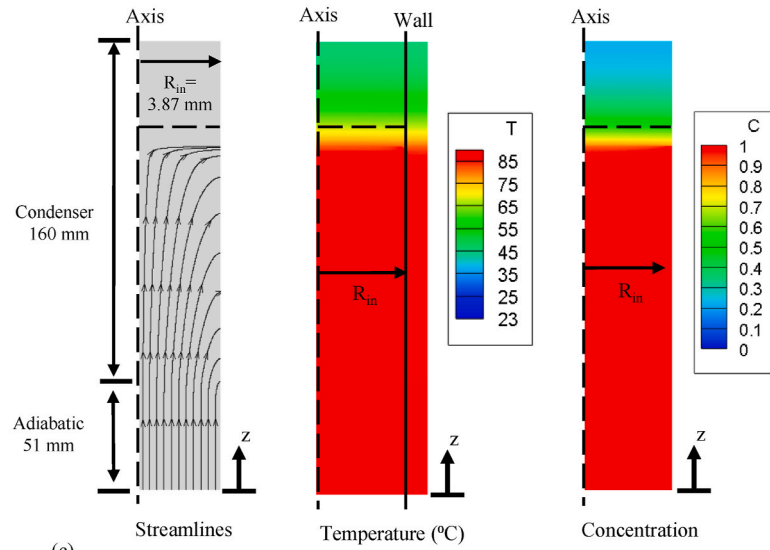
For the six test cases investigated experimentally, the wall temperatures measured along the tube is shown in Fig. 4(a)-(b). Fig. 4(a) shows the wall temperature distribution for the forced convection test cases with methanol temperatures between 66.70 °C and 86.92 °C. If we look at the test case with $T = 86.92$ °C, we can see that the temperatures are initially uniform in the adiabatic and the condenser sections. Then at a specific point in the condenser section, a steep drop in temperature occurs. This point marks the location of the two-phase interface between the vapor and NCG. This is caused by the significantly lower heat transfer rate in the NCG region. This general trend stays the same for the two other test cases with $T = 77.02$ °C and $T = 66.70$ °C. The difference being the shift in the location of the interface towards the adiabatic section as we lower the temperatures. This is because as shown in Table 2, a lowering of the working fluid temperature, reduces the operating pressure, and that decompresses the NCG. Thus, there is a reduction in the condensation length with the interface moving closer to the adiabatic section. This moving of the interface location, also captured experimentally, is one of the most important benefits of a gas-charged thermosyphon or a variable conductance heat pipe where the



(a)



(b)



(c)

(caption on next page)

Fig. 7. CFD simulation results for natural convection test cases with (a) working temperature of 68.0 °C, (b) working temperature of 78.04 °C, and (c) working temperature of 87.32 °C.

system self-adjusts its condensation length based on the evaporator heat input or the operating temperature. Similarly, Fig. 4(b) shows the wall temperature variation for the natural convection test cases with methanol temperatures between 68.00 °C and 87.32 °C. Similar trends as that observed in forced convection are seen here as well. Overall, the trends in temperature between natural convection and forced convection are similar in the adiabatic and condenser regions for the corresponding working fluid temperatures with the temperature remaining uniform until the two-phase interface. Even though the interface location is the same, the net rate of heat transfer is lower in the natural convection test cases leading to a higher wall temperature in the NCG region in comparison to the forced convection test cases.

Fig. 5(a) and (b) shows wall temperature contour images captured by the IR camera and the corresponding thermocouple measurement for two test cases at the lowest temperatures in forced convection ($T = 66.70$ °C) and natural convection ($T = 68.00$ °C), respectively. In general, the trends along the axis are captured reasonably well, qualitatively; however, an exact comparison with the thermocouple data is not made because the IR image cannot focus on a curved surface the same way as it can do with a flat surface. The curvature of the image causes the centerline temperature, where the camera is focused, to be different in comparison with the edges.

4.2. Computational model results

Fig. 6(a)-(c) shows the simulation results for all three forced convection test cases with methanol temperatures between 66.7 °C and 86.92 °C. For the test case with an operating temperature of $T = 66.7$ °C, Fig. 6(a) shows the CFD domain results for velocity streamlines, local temperature variation, and phase concentration. The location of the interface has been marked at a concentration value of 0.5 in all these images. The velocity streamlines show how the flow entering the adiabatic section from the bottom region and condensing along the wall. Because we are simulating a phase transfer at the wall, the velocity contour results show a disappearance of the vapor at the wall signifying condensation to the liquid phase. The temperature distribution shows the temperature being almost steady and being very close to saturation in the adiabatic and condenser region until the two-phase interface. The drop in temperature to ambient conditions occurs in the NCG region because there is very low heat transfer in this domain with wall temperatures being close to T_{∞} . The corresponding concentration distribution shows the existence of complete vapor in the bottom section and complete NCG in the top section, while the two-phase interface is diffused having a thickness which is a result of the selected diffusion coefficient between the two phases. Fig. 6(b) and (c) show the simulation results for the two other methanol working temperature test cases with $T = 77.02$ and 86.92 °C, respectively. While a similar trend as that was seen for $T = 66.7$ °C is observed, the interface location is shifted as expected for higher operating temperatures, leading to higher pressures, and so compressed NCG regions. This behavior follows the same trends observed in the experiments showing that the CFD results are able to capture the fluid flow behavior reasonably well.

Fig. 7(a)-(c) shows the simulation results for all three forced convection test cases with methanol temperatures being 66.7 °C, 77.02 °C, and 86.92 °C. For the test case with an operating temperature of $T = 66.7$ °C, Fig. 7(a) shows the CFD domain results for velocity streamlines, local temperature variation, and phase concentration. Overall, the behavior in the adiabatic and condenser region until the two-phase interface is the same as that observed in the forced convection test case with $T = 66.7$ °C. The main differences being the net vapor flow rate is much lower for the natural convection test case and the NCG phase temperatures and the corresponding wall temperature across the interface are higher due to a lower rate of heat transfer in this configuration. Fig. 7(b) and (c) follow similar behavior and trends, with the upward shift in interfacial location caused by the higher operating temperatures.

4.3. Model validation

While not all parameters could be directly compared between the experiments and the simulations, the measured and predicted wall temperature variation is the one parameter that can be used for model validation. Fig. 8 shows a comparison of the experimental data and the simulation result for the three forced convection test cases with $T = 66.7$ °C, 77.02 °C, and 86.92 °C. The mean absolute error (MAE) to compute the predicting accuracy of the CFD model is defined as

$$MAE = \frac{1}{N} \sum \left| \frac{T_{CFD,i} - T_{exp,i}}{T_{exp,i}} \right|, \quad (13)$$

where i is the local axial thermocouple location. For the forced convection test cases, the MAE was 3.09%, showing that the CFD predictions agree reasonably well with the experimentally measured wall temperatures. Both experimental data and CFD results follow the same general trend with steady temperature variation in the adiabatic and condenser region until the two-phase interface and a steep drop in the NCG region. While the interface location is captured well with the temperature starting to drop at almost the same location in both situations, the variation in the NCG region is slightly different. The main reason for this difference is that in the real scenario, we can expect a slight rate of condensation to occur even in the NCG domain due to vapor diffusion, that is not being currently captured by the simulations.

Fig. 9 shows a comparison of the experimental data and the simulation result for the three forced convection test cases with $T = 68.0$ °C, 78.04 °C, and 87.32 °C. The MAE for the natural convection test cases is 3.52%. In general, similar to the test cases for forced convection, the simulations are able to capture the wall temperature variation observed in the experiments to a good degree. Here, even the variation across the two-phase interface is captured better than what was observed for the forced convection test cases. The

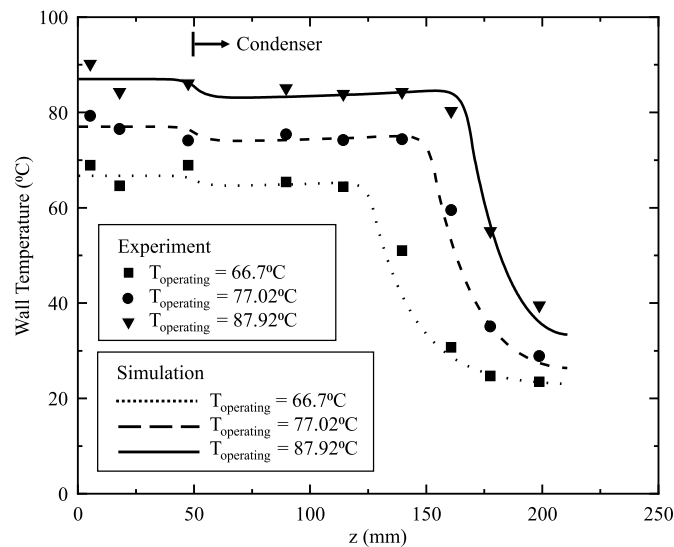


Fig. 8. Forced convection test cases comparison between experimental data and simulations.

main reason for this is that the rate of heat transfer is significantly lower in comparison to the forced convection test cases, reducing the impact of wall condensation on heat transfer and corresponding wall temperature variation across the interface.

With this validation effort, we developed a CFD model for predicting the heat transfer and fluid flow inside a variable conductance thermosyphon. Overall, the results of this study show extremely good predicting accuracy of this CFD model for a range of operating conditions of the experiment, making it a possible predicting tool for variable conductance thermosyphon configurations that thermal engineers can use to make critical design decisions.

5. Conclusion

This study investigated experimentally and computationally, a variable conductance heat pipe operating in the vertical orientation. A variable conductance thermosyphon experiment was set up to perform a heat transfer investigation with methanol as the working fluid and argon as the NCG. Forced convection air flow and natural convection air flow conditions were tested on the condenser domain of the variable conductance thermosyphon. Experimental thermocouple data for both forced convection and natural convection test cases show temperature remaining almost uniform in the adiabatic section and dropping rapidly across the vapor/NCG interface between the vapor and NCG. An in-house CFD code was developed in Fortran to predict the fluid flow and heat transfer utilizing a 2D axisymmetric computational domain with a diffused interface between the vapor and NCG domains. The CFD model predicts the wall temperature data observed experimentally in both forced convection and natural convection test cases with good accuracy. With this CFD model, we develop a new computational framework for predicting the heat transfer and fluid flow inside a variable conductance thermosyphon that can in the future become an extremely useful tool for thermal design engineers.

CRediT author statement

Cho-Ning Huang: Methodology, Software, Validation, Investigation, Writing - original draft. **Kuan-Lin Lee:** Formal Analysis, Validation, Writing - review & Editing. **Calin Tarau:** Methodology, Validation, Resources. **Yasuhiro Kamotani:** Conceptualization, Methodology, Software, Supervision, Writing - review & Editing. **Chirag R. Kharangate:** Conceptualization, Methodology, Supervision, Writing - original draft, Writing - review & Editing.

Declaration of competing interest

The authors declare that they have no known competing financial interests or personal relationships that could have appeared to influence the work reported in this paper.

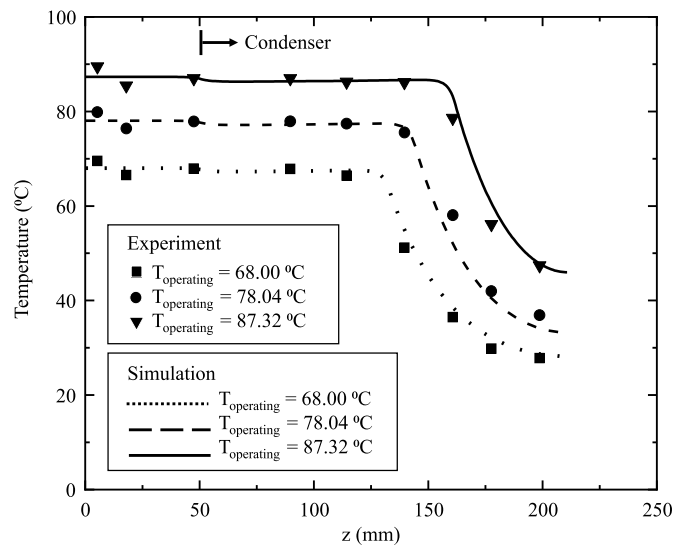


Fig. 9. Natural convection test cases comparison between experimental data and simulations.

Acknowledgment

This project was sponsored by NASA Marshall Space Flight Center (MSFC) under an STTR Phase I program (Contract# 80NSSC18P2155). We would like to thank the program manager, Brian O'Connor, and Dr. Jeff Farmer for their supports and valuable inputs during the program. We also would like to thank Philip Texter, Chris Jarmoski, and Cheyenne Jones for their significant technical contributions to this program.

This work made use of the High Performance Computing Resource in the Core Facility for Advanced Research Computing at Case Western Reserve University.

References

- [1] I. Mudawar, Recent advances in high-flux, two-phase thermal management, *J. Therm. Sci. Eng. Appl.* 5 (2013), <https://doi.org/10.1115/1.4023599>.
- [2] A. Faghri, Review and advances in heat pipe science and technology, *J. Heat Tran.* 134 (2012).
- [3] Y. Lee, U. Mital, A two-phase closed thermosyphon, *Int. J. Heat Mass Tran.* 15 (1972) 1695–1707, [https://doi.org/10.1016/0017-9310\(72\)90098-1](https://doi.org/10.1016/0017-9310(72)90098-1).
- [4] K.-L. Lee, C. Tarau, A. Lutz, W.G. Anderson, C.-N. Huang, C. Kharangate, Y. Kamotani, Advanced hot reservoir variable conductance heat pipes for planetary landers, in: 50th International Conference on Environmental Systems (ICES 2020), Virtual Event, 2020.
- [5] B.D. Marcus, Theory and Design of Variable Conductance Heat Pipes, 1972.
- [6] M. Shiraiishi, K. Kikuchi, T. Yamanishi, Investigation of heat transfer characteristics of a two-phase closed thermosyphon, *J. Heat Recovery Syst.* 1 (1981) 287–297, [https://doi.org/10.1016/0198-7593\(81\)90039-4](https://doi.org/10.1016/0198-7593(81)90039-4).
- [7] H. Imura, K. Sasaguchi, H. Kozai, S. Numata, Flux thermique critique dans un thermosyphon ferme et diphasique, *Int. J. Heat Mass Tran.* 26 (1983) 1181–1188, [https://doi.org/10.1016/S0017-9310\(83\)80172-0](https://doi.org/10.1016/S0017-9310(83)80172-0).
- [8] H. Li, A. Akbarzadeh, P. Johnson, The thermal characteristics of a closed two-phase thermosyphon at low temperature difference, *Heat Recovery Syst. CHP* 11 (1991) 533–540, [https://doi.org/10.1016/0890-4332\(91\)90055-9](https://doi.org/10.1016/0890-4332(91)90055-9).
- [9] H. Hashimoto, F. Kaminaga, Heat transfer characteristics in a condenser of closed two-phase thermosyphon: effect of entrainment on heat transfer deterioration, *Heat Tran. Asian Res.* 31 (2002) 212–225, <https://doi.org/10.1002/htj.10030>.
- [10] S.H. Noie, Heat transfer characteristics of a two-phase closed thermosyphon, *Appl. Therm. Eng.* 25 (2005) 495–506, <https://doi.org/10.1016/j.applthermaleng.2004.06.019>.
- [11] H. Jouhara, A.J. Robinson, Experimental investigation of small diameter two-phase closed thermosyphons charged with water, FC-84, FC-77 and FC-3283, *Appl. Therm. Eng.* 30 (2010) 201–211, <https://doi.org/10.1016/j.applthermaleng.2009.08.007>.
- [12] E. Gedik, Experimental investigation of the thermal performance of a two-phase closed thermosyphon at different operating conditions, *Energy Build.* 127 (2016) 1096–1107, <https://doi.org/10.1016/j.enbuild.2016.06.066>.
- [13] C. Harley, A. Faghri, Complete transient two-dimensional analysis of two-phase closed thermosyphons including the falling condensate film, *J. Heat Tran.* 116 (1994) 418–426, <https://doi.org/10.1115/1.2911414>.
- [14] J. Legierski, B. Więcek, G. De Mey, Measurements and simulations of transient characteristics of heat pipes, *Microelectron. Reliab.* 46 (2006) 109–115, <https://doi.org/10.1016/j.microrel.2005.06.003>.
- [15] B. Jiao, L.M. Qiu, X.B. Zhang, Y. Zhang, Investigation on the effect of filling ratio on the steady-state heat transfer performance of a vertical two-phase closed thermosyphon, *Appl. Therm. Eng.* 28 (2008) 1417–1426, <https://doi.org/10.1016/j.applthermaleng.2007.09.009>.
- [16] A. Alizadehdakheel, M. Rahimi, A.A. Alsairafi, CFD modeling of flow and heat transfer in a thermosyphon, *Int. Commun. Heat Mass Tran.* 37 (2010) 312–318, <https://doi.org/10.1016/j.icheatmasstransfer.2009.09.002>.
- [17] B. Fadhl, L.C. Wrobel, H. Jouhara, Numerical modelling of the temperature distribution in a two-phase closed thermosyphon, *Appl. Therm. Eng.* 60 (2013) 122–131, <https://doi.org/10.1016/j.applthermaleng.2013.06.044>.
- [18] B. Fadhl, L.C. Wrobel, H. Jouhara, CFD modelling of a two-phase closed thermosyphon charged with R134a and R404a, *Appl. Therm. Eng.* 78 (2015) 482–490, <https://doi.org/10.1016/j.applthermaleng.2014.12.062>.
- [19] H. Shabgard, B. Xiao, A. Faghri, R. Gupta, W. Weissman, Thermal characteristics of a closed thermosyphon under various filling conditions, *Int. J. Heat Mass Tran.* 70 (2014) 91–102, <https://doi.org/10.1016/j.ijheatmasstransfer.2013.10.053>.
- [20] D. Jafari, A. Franco, S. Filippeschi, P. Di Marco, Two-phase closed thermosyphons: a review of studies and solar applications, *Renew. Sustain. Energy Rev.* 53 (2016) 575–593, <https://doi.org/10.1016/j.rser.2015.09.002>.

- [21] M. Ramezanizadeh, M. Alhuyi Nazari, M.H. Ahmadi, E. Açıkkalp, Application of nanofluids in thermosyphons: a review, *J. Mol. Liq.* 272 (2018) 395–402, <https://doi.org/10.1016/j.molliq.2018.09.101>.
- [22] M. Ramezanizadeh, M. Alhuyi Nazari, M.H. Ahmadi, K. wing Chau, Experimental and numerical analysis of a nanofluidic thermosyphon heat exchanger, *Eng. Appl. Comput. Fluid Mech.* 13 (2019) 40–47, <https://doi.org/10.1080/19942060.2018.1518272>.
- [23] A.R. Rohani, C.L. Tien, Steady Two-Dimensional Heat and Mass Transfer in the Vapor-Gas Region of a Gas-Loaded Heat Pipe, ASME Pap, 1972.
- [24] R. Ponnappan, Studies on the Startup Transients and Performance of a Gas Loaded Sodium Heat Pipe, UNIVERSAL ENERGY SYSTEMS INC DAYTON OH, 1989.
- [25] G. Harley, A. Faghri, Transient two-dimensional gas-loaded heat pipe analysis, *J. Heat Tran.* 116 (1994) 716–723, <https://doi.org/10.1115/1.2910927>.
- [26] K.L. Lee, J.R. Kadambi, Y. Kamotani, The influence of non-condensable gas on an integral planar heat pipe radiators for space applications, *Int. J. Heat Mass Tran.* 110 (2017) 496–505, <https://doi.org/10.1016/j.ijheatmasstransfer.2017.03.060>.
- [27] S. Sichamnan, T. Chompookham, T. Parametthanuwat, A case study on internal flow patterns of the two-phase closed thermosyphon (TPCT), *Case Stud. Therm. Eng.* 18 (2020) 100586, <https://doi.org/10.1016/j.csite.2020.100586>.
- [28] C. Enke, J. Bertoldo Júnior, V. Vlassov, Transient response of an axially-grooved, aluminum-ammonia heat pipe with the presence of non-condensable gas, *Appl. Therm. Eng.* 183 (2021) 116135, <https://doi.org/10.1016/j.applthermaleng.2020.116135>.
- [29] F.P. Incropera, D.P. Dewitt, T.L. Bergman, A.S. Lavine, Fundamentals of Heat and Mass Transfer, John Wiley, Hoboken, NJ, 2002, pp. 939–940, 1985.
- [30] R.C. Roberts, Molecular Diffusion of Gases, 1963, pp. 2–249.
- [31] R. Hilpert, Heat transfer from cylinders, *Forsch. Geb. Ingenieurwes.* 4 (1933) 215.
- [32] A.J. Ede, Advanced in natural convection, *Adv. Heat Tran.* 4 (1967).
- [33] S. V Patankar, Numerical Heat Transfer and Fluid Flow, Publ. Corp., Washington DC, 1980. Hemisphere.